Check for updates

View Article Online
View Journal

Nanoscale Advances

Accepted Manuscript

This article can be cited before page numbers have been issued, to do this please use: R. Pandillapally, J. Pillanagrovi, S. Dutta-Gupta and S. Duraiswamy, *Nanoscale Adv.*, 2026, DOI: 10.1039/D5NA01087J.

This is an Accepted Manuscript, which has been through the Royal Society of Chemistry peer review process and has been accepted for publication.

Accepted Manuscripts are published online shortly after acceptance, before technical editing, formatting and proof reading. Using this free service, authors can make their results available to the community, in citable form, before we publish the edited article. We will replace this Accepted Manuscript with the edited and formatted Advance Article as soon as it is available.

You can find more information about Accepted Manuscripts in the Information for Authors.

Please note that technical editing may introduce minor changes to the text and/or graphics, which may alter content. The journal's standard Terms & Conditions and the Ethical guidelines still apply. In no event shall the Royal Society of Chemistry be held responsible for any errors or omissions in this Accepted Manuscript or any consequences arising from the use of any information it contains.

ROYAL SOCIETY OF CHEMISTRY

rsc.li/nanoscale-advances

View Article Online
DOI: 10.1039/D5NA01087J

ARTICLE

Real-Time Optical Spectroscopy for *In-situ* Single Droplet Analysis

Received 00th January 20xx,
Accepted 00th January 20xx

DOI: 10.1039/x0xx00000x

Rama Pandillapally[a], Pillanagrovi Jayakumar [b], Shourya Dutta-Gupta[b*] and Suhanya Duraiswamy[a*]

In-situ monitoring of chemical reactions specifically reactions leading to the formation of plasmonic nanomaterials within droplets, has become a necessity for several applications in nanotechnology, and sensing. In this study, we use a custom-designed optical transmission spectroscopy setup that can detect signals from a single anisotropic droplet over the entire visible spectral range (400 – 900 nm) without the use of external additives as reporters. We use data obtained from the light scattered from droplets to differentiate the 'drop only' regions from the 'oil only' regions and extract information from within single drops. We then load the droplets with anisotropic gold nanoparticles of different concentrations and show the variations in the optical signals based on their concentraions, from single drop, and compare the data to the averaged data from several drops, to demonstrate the validity of our technique. Finally, we employ the developed platform for monitoring *in-situ* synthesis of gold nanoparticles within the microfluidic chip in real time. Measurement at different locations along the channel enables us to track the reaction within a drop at different time points, providing insights into the reaction kinetics. We also measure spectral data to understand the influence of reagent concentration on the synthesis. The developed technique thus can be employed for *in-situ* monitoring of any chemical reaction within a single anisotropic drop, provided they have absorption/transmission signatures and will find wide applicability in the development of single droplet analysis platforms.

Introduction

Droplet microfluidics involves the controlled formation and transport of nanolitre to picolitre sized drops in an immiscible phase (typically oil) and are often used in applications involving highly parallelized and precise measurements[1]. Typically, drops have been employed as micro-controlled reactors (reaction/assay chambers) since each miniaturized drop (lengths ~ nm to µm) can be regulated and operated independently[2–4]. Pump-controlled reagent dispensing procedure imparts precise control over the reagent volumes in individual drops, since it is automated; while chaotic advection within each droplet enables identical mixing patterns within them, thus ensuring robust and reproducible assays with improved reaction kinetics and without significant batch-to-batch variations[5]. Current research focus in the droplet microfluidics arena is towards building capabilities to independently manipulate and monitor each droplet, which will, in-turn, enable the identification of reaction mechanisms, crystal structures and biochemical pathways leading to pathological and physiological changes in the cell[6], tissue and/or organs.

Real-time monitoring of individual droplets and recognizing the variations in successive droplets, over time is a significant challenge. Real-time monitoring provides vital information about reaction mechanisms and biochemical pathways and can also be used to effectively and efficiently modify and manipulate parameters to achieve desired results. Researchers have explored various approaches for real-time monitoring by integrating mass spectroscopy[7], electrochemical[8], and optical[9] platforms with microchannels to analyse individual drops over a period of time. Each method of monitoring has its advantages as well as limitations. For example, when using electrochemical monitoring techniques, measuring the presence of small molecules like H_2O_2 by appropriate coupling with a redox reaction is possible. However, in this case the microfluidic device must be integrated with electrodes to carry out electrical measurements. On the other hand, mass spectroscopic approaches provide unparalleled sensitivity and specificity, owing to the unique signatures observed in the mass spectrum. However, this is a destructive technique that results

[a.] *Chemical Engineering, Indian Institute of Technology Hyderabad, Sangareddy 502284, Telangana, India*
[b.] *Materials Science and Metallurgical Engineering, Indian Institute of Technology Hyderabad, Sangareddy 502284, Telangana, India*
*Corresponding author email: shourya@msme.iith.ac.in and suhanya@che.iith.ac.in
Supplementary Information available: [details of any supplementary information available should be included here]. See DOI: 10.1039/x0xx00000x

Open Access Article. Published on 20 January 2026. Downloaded on 1/22/2026 7:56:22 AM.
This article is licensed under a Creative Commons Attribution-NonCommercial 3.0 Unported Licence.

Nanoscale Advances Accepted Manuscript

View Article Online
DOI: 10.1039/D5NA01071

Open Access Article. Published on 20 January 2026. Downloaded on 1/22/2026 7:56:22 AM.
This article is licensed under a Creative Commons Attribution-NonCommercial 3.0 Unported Licence.

Nanoscale Advances Accepted Manuscript

in loss of the prepared sample. In contrast, monitoring single drop through their optical signatures opens up avenues for non-destructive and non-invasive detection of various species in the drop. Optical interrogation techniques of a drop have been used for single-cell analysis, biochemical, molecular detection, and cell sorting[10,11] due to their high sensitivity, fast response, and ease of integration with microreactors[12].

Optical interrogation techniques deal with methods where light is absorbed, emitted, or dispersed by a sample (droplet in this case or sample within the droplet) to access its properties such as composition, structure, electrical and/or vibrational[13–18]. In such cases, the microfluidic chip is integrated with optical component directly by aligning the optical path with the channel through which drops flow and the detector collects the signals which are processed to obtain the corresponding signatures. Optical interrogation can be performed by monitoring modulations in optical signals (like transmission, absorption, scattering, fluorescence and Raman scattering) as a function of flow parameters within a single droplet[19,20]. Raman and fluorescent spectroscopy have been integrated with droplet microfluidics for carrying out single droplet analysis[21–24]. For example, Cecchini *et al.* reported the aggregation of silver nanoparticles in droplet microfluidics using the Raman reporter malachite green (MG) with an exposure time of 10 µs [25,26] while fluorescent detection methods have been reported by *Casadevall et al*[23]. Both the methods capture inelastic scattered signals and high signal to noise (S/N) ratios are possible due to the efficient filtering using filter cubes. However, in both these cases a Raman reporter or a fluorescing molecule needs to be added to the aqueous solution to enable detection[27,28].

Several absorbance-based detectors have been reported in the literature for glucose detection, single cell analysis and enzymatic reactions[29–31]. However, these methods are limited to the study of large droplets due to the inherent short optical pathlength at the single droplet level. This limitation has been addressed recently: Duncombe *et al.* demonstrate an UV-Vis absorption spectrum-based droplet sorter wherein they acquire a broadband spectrum (200 – 1050 nm) at 2100 spectra per second in a microchip. Their devices had implanted waveguides (optical fiber inserted on either side of the region of interest) enabling excellent spatial and temporal localized measurements within the channels. However, this configuration limits the ability to choose the point of interrogation along the channel length, restricting the use of the proposed detection scheme for time-dependent processes such as reaction kinetics analysis[32].

Probst *et al*. established a sensitive technique that was able to acquire complete absorption spectra from a single pL droplet by using a fast spectrometer for integration times as short as 50 µs per spectrum. Additionally, they also used a postprocessing algorithm that improves the (S/N) ratio by removing the spectra of oil (by using single wavelength time trace at 405 nm since the fluorinated oil had a higher absorbance than the aqueous phase). They then examined the salt-induced aggregation of spherical nanoparticles in single spherical droplet. They initially used fluorescein isothiocyanate to test their method and were able to determine 800 nM concentrations of the fluorescent molecules in the droplet[33]. They then used the same technique to show the detection of spherical gold nanoparticles (GNP) in droplets. The reported method was used for measuring the signatures of preformed GNPs (off-chip synthesis) in spherical droplets, and their salt induced aggregations.

Sulliger *et al.* recently proposed an optofluidic platform consisting of hyperspectral imaging (HSI) using a 4*f* imaging platform integrated with a microfluidic channel to identify and sort single drops of volume ~ 0.5 pL. They constructed a modular setup using a 4*f* imaging system with 4x objective in order to measure the spectra from a train of droplets. In particular, they showed that the presence of index matching between the droplet and the oil could enable the measurement of around 75% of the plug shaped droplets. Using this system they showed the detection of gold nanoparticles (spherical and nanorods) as well as DNA mediated dimer formation within the droplets (no chemical reactions). They showed a detection limit of 6 AuNP/droplet, temporal time resolution of 2 ms which could further be improved to 500 µs with a lower S/N ratio[34].

It should be noted that the NA of the objective decides the angular range of the collected forward-scattered signal. Therefore, by tuning the NA of the collection objective, it is possible to measure either the extinction signal (low NA) or a convolution of extinction and scattered signals (high NA). Both Probst *et al.* and Sulliger *et al.* have tailored the continuous phase[33,34], by using fluorinated oil of higher absorbance in the former and index matched oil in the latter to improve the S/N ratios which is typically not feasible in many cases involving chemical reactions (inert oil is preferred). Hence it is prudent to study systems where there is non-negligible scattering from droplet edges in the context of single-droplet measurements.

In addition, when dealing with chemistries in droplets, the channel geometry, channel material the choice of continuous phase and the flow rate ratios between the continuous and dispersed phase plays an important role. Typical geometries employed for microfluidic drop generation are the "flow focusing" and/or "T-junction geometries" in traditional PDMS-based microfluidics[35]. The sizes of the aqueous droplets of the dispersed phase formed in the continuous oil phase in these geometries are modified by varying the flow rates of the two fluids (oil and/or aqueous) with respect to each other. These variation in the flow ratios of the fluids alters the inertial forces, viscous forces and interfacial forces between the fluids given by the Reynolds number $(Re = D v \rho / \mu)$ and the

This journal is © The Royal Society of Chemistry 20xx

Please do not adjust margins

View Article Online
DOI: 10.1039/D5NR01887F

capillary number $(Ca = \mu v/\sigma)$ where v, μ and ρ are the velocities, viscosities and densities respectively of either the continuous fluid or dispersed fluid depending on the fluid considered in the evaluation, D the characteristic dimension of the microchannel and σ the interfacial tension between the two fluids. The opposing viscous shear and interfacial forces between the continuous phase and advancing dispersed phase leads to droplet breakup at the junction[36,37]. For example, spherical droplets of varying dimensions are typically formed in a flow focusing junction where the narrow necking geometry contributes to the droplet formation in addition to the favourable Re and Ca. This geometry is preferred only in case of slow reactions, requiring high frequency droplets as in the case of droplet polymerase chain reactions (dPCR)[38], organoids and spheroids for 3D cultures and for bioassays that look at large volume collection and monitoring over a period of time[39,40]. These geometries are generally not preferred for chemical reactions that are kinetically controlled since such reactions will typically lead to fouling and flow disruption at the narrow necking junction, as also shown by us in the Figure S1 of Supplementary information (SI, details in the Droplet generation in the microfluidic chip section of Methods and Materials).

T-junction geometries have orthogonal channels where the dispersed phase meets the continuous phase flowing along a long primary channel at a 'T'. The breakup mechanism involves only the interplay between the three above-mentioned forces represented in terms of Re and Ca leading to droplets of varying shapes depending on the flowrate regimes, including spherical, bullet shaped (with a narrow leading edge and a wider trailing edge), capsule shaped droplet (with wide leading and trailing edges) as well as other irregular shaped drops[41–45]. T-junction is the preferred geometry for chemical reactions involving droplets and/or reactions involving material exchange between the dispersed and continuous phase and segmented flow[39,40,46–49].

Given a particular geometry, the shape and size of the droplets are modified by changing the flow rates of the aqueous fluid (Q_a) and the continuous phase fluid/oil (Q_o) i.e. by adjusting their flow rate ratios, $R = Q_a/Q_o$. However, since flow ratios are dependent on the final concentrations of the reagents for reaction chemistry, the effective range of flow ratios that can be used without affecting the final concentrations in the drops is in most cases very limited. Hence, essentially the droplet shape is process dependant - this leads to employing anisotropic drop shapes in most droplet microreactors; Thus, for application-based droplet microflow processes, the droplet shape cannot be dictated by the analysis method which implies *that single-drop analysis methods need to cater to droplets of any shape and size.*

This has also been highlighted by a recent work by Zanini *et al.* where they explain the effects of light illumination on the ellipsoidal droplet in the squeezing, dripping-squeezing transition, and dripping regimes in rectangular channels both experimentally and using theoretical simulations[50]. They then go on to show the best microfluidic configuration with high signal detection regions emphasizing the fact that optical interrogation of spherical droplets significantly reduces the applicability of such methods to real processes. However, in their study, they used an in-plane optical interrogation through a waveguide illumination which intrinsically leads to the droplet being illuminated with a divergent beam that has different light-droplet interactions. Furthermore, the in-plane illumination geometry severely limits the types of chips that can be integrated with this online platform.

In this article, we develop an approach for monitoring single drops (bullet and capsule-shaped drops formed in T-junction geometry) by integrating a microfluidic droplet system with a customized optical setup developed in the lab. In particular, we measure the forward scattered optical signal to study the evolution of signals arising from single drops. In the first part of the article, we explain the developed platform and the associated data analysis used for extracting the single droplet information. Subsequently, we employ this technique to study the presence of gold nanoparticles within single drops. We also study the in-situ synthesis of gold nanoparticles demonstrate the versatility of the proposed technique for the analysis of single drops on the fly within microfluidic flow systems. *This is the first demonstration of optical interrogation of a single drop with chemical reaction leading to the synthesis of gold nanoparticles.*

Materials and Methods

Materials

Sodium borohydride ($NaBH_4$, 98%), Hydrogen tetrachloroaurate (III) trihydrate ($HAuCl_4 \cdot 3H_2O$, 99.99%), Hexadecyltrimethyl ammonium bromide (CTAB, 99%), Silver nitrate ($AgNO_3$, 99.9% of Ag) and L-(+)-ascorbic acid (AA, 99%) were purchased from SRL Co. Ltd. Silicon oil (99%, viscosity of 10 cst) was purchased from Taranath Scientific limited. Additionally, ultrapure deionized (DI) water with a resistivity of 18 MΩ-m was used for all experiments. Note that high-purity water was used to avoid contamination and was crucial in ensuring repeatable results.

Microfluidic chip fabrication

SU-8 master patterns on silicon wafers were used as templates for PDMS (Sylgard 184, Kevin Electrochem, India) device fabrication. Briefly, the PDMS base and curing agent were mixed in 10:1 ratio and poured over the master pattern, degassed and was allowed to cure at 70 °C for 2 hrs. The cured PDMS slab was then peeled off from the silicon template, inlet/outlet holes punched, cleaned and bonded to a PDMS

Open Access Article. Published on 20 January 2026. Downloaded on 1/22/2026 7:56:22 AM.
This article is licensed under a Creative Commons Attribution-NonCommercial 3.0 Unported Licence.

Nanoscale Advances Accepted Manuscript

Please do not adjust margins

View Article Online
DOI: 10.1039/D5NA01087F

Open Access Article. Published on 20 January 2026. Downloaded on 1/22/2026 7:56:22 AM.
This article is licensed under a Creative Commons Attribution-NonCommercial 3.0 Unported Licence.

coated glass slides after 40 s of plasma treatment (Harrick plasma PDC-32G-2, USA). Tubings (FEP, Vici, India) of inner and outer diameters 0.8 mm and 1.5 mm respectively were fixed to the inlet/outlet holes and glued using epoxy (Devcon, India). The microchannels used in this study were rectangular in cross-section and were 300 µm wide, 155 µm deep, and 4.5 cm long. The layout of the microfluidic chip is shown in Figure S2 of SI.

Droplet generation in the microfluidic chip

As mentioned previously, we also used flow focusing (FF) geometry of two different dimensions, to generate drops for gold nanomaterial synthesis, as shown in Figure S1 of SI. The dimensions of the narrow necking zone of device in images shown in Figures S1A and S1B are 50 µm width and 150 µm length and depth while that in Figures S1C – S1F are 200 µm width and 200 µm length and depth. The continuous fluid (silicone oil) flows through channels marked 'oil' and the dispersed fluid (an aqueous solution of gold salt and ascorbic acid, the reducing agent), flows in through the inlets marked 'Aqueous' respectively. Figure S1A corresponds to 'only water' experiment which leads to isotropic drops forming at the junction. For gold nanoparticle synthesis, gold salt (0.5 mM) and reducing agent (ascorbic acid at 0.5 M and 1 M considered to be a slow reducing agent for gold salt), were flown in through 2 different inlets, meeting just near the narrow neck. As can be seen in all the gold nanomaterial synthesis experiments (Figures S1B - S1F), there are deposits on the channel which leads to channel fouling and flow disruption. Hence, we use Tjunction geometry in this study.

In this study, we used T-junction microfluidic device that comprises three inlets of dimension. Silicon oil was pumped through the inlet 1, as shown in Figure S2 of SI and water through inlet 2 (Figure S2 of SI) using a syringe pump (Chemyx, USA). The third inlet (GNR in Figure S2 of SI) was used for the experiments performed with gold nanorods only and was blocked for other experiments. The microfluidic chip was placed under a stereomicroscope (Nikon SMZ1270) and the drops formed in the channel were imaged for different flowrates of oil and water. Table S1 of SI lists the flow rates, corresponding velocities and flow ratios used in the experiments. The images were then processed using ImageJ to determine the dimensions of the generated droplets.

Gold nanorod synthesis

Gold nanorods (GNR) were synthesized using the seed mediated growth method proposed by Nikoobakht and El-Sayed[51]. Briefly, seeds were synthesized by adding a freshly prepared ice-cold $NaBH_4$ (0.6 mL of 0.01 M) to a mixture of aqueous $HAuCl_4{\cdot}3H_2O$ (10 mL of 0.5 mM) and CTAB (10 mL of 200 mM) solution. The mixture was vigorously stirred for 2 min, until the colour of the solution turned brown indicating the formation of seeds of size ~4 nm. Freshly prepared seeds were further used for the growth of GNR by adding growth solution (1 mM $HAuCl_4$, 0.2 M CTAB and 4mM $AgNO_3$) to 70 mL of AA (0.078M). 12 mL of the freshly prepared seed solution was then added to the colourless solution and kept undisturbed for 20 min for the growth of the GNRs. The as-prepared samples were then characterized using UV-Visible spectroscopy (Shimadzu UV-1780) and TEM (JEOL F200FS, operated at 200 KV).

Modelling light scattering by droplets

The light scattering by single drops was calculated using ray tracing method[52]. Here, each aqueous droplet (refractive index of 1.33) was embedded in a homogenous background of oil (refractive index of 1.45). The droplet was illuminated with a localized collimated light source mimicking the illumination condition used in the experiments. The forward scattered light was detected by placing a detector (with an angular range of 70°). Note that in the experiments, a 60X air immersion objective (NA of 0.7) was used, which corresponds to a collection angle of 44°. The position of the illumination source and the detector were kept fixed, whereas the droplet is moved relative to them. This enabled us to study the changes in the forward scattering as the light from the source illuminates different parts of the droplet.

Optical transmission spectroscopy

A homemade optical setup was used for all the real-time optical spectroscopic measurements. Briefly, the system consisted of an inverted optical microscope (Nikon Ti2U) coupled to an optical spectrometer (Andor Kymera 328i with Newton 920 CCD). The microfluidic chip was illuminated with a halogen light source through a condenser lens (NA of 0.52). Area of the light illumination was 0.5 μm^2. The condenser aperture was tuned to choose the illuminated region of the droplet. The transmitted light was collected using a 60X, 0.7 NA air immersion objective and analysed by the spectrometer. The spectrometer could acquire a spectrum with 3 ms acquisition time and operated at 3 MHz rates to acquire the maximum number of spectra from a given droplet. The spectrometer acquisition parameters like integration time, repetition rate, clock speed were adjusted such that a maximum data throughput for a single drop was achieved. It should be noted that this is primarily limited by the dark current and the noise level of the CCD in the spectrometer. For a droplet with length of 600 µm, an integration time of 3 ms, ensures that over a period of 30 s cumulative time, we acquired 8200 spectra and measured the spectra from 25 distinct drops. A similar trend is expected for droplets with smaller dimensions (≈ 40 µm) as well.

Data analysis

Nanoscale Advances Accepted Manuscript

This journal is © The Royal Society of Chemistry 20xx

Please do not adjust margins

View Article Online
DOI: 10.1039/D5NA01087J

Open Access Article. Published on 20 January 2026. Downloaded on 1/22/2026 7:56:22 AM.
This article is licensed under a Creative Commons Attribution-NonCommercial 3.0 Unported Licence.

We recorded ~5000-8000 spectra for a single flow condition, using the customized optical spectroscopy setup. Each spectrum was recorded with a 3 ms acquisition time. The relative transmission intensity was derived by normalizing the raw spectrum with the spectrum from the bulk PDMS chip (without the flow channel). The dark current was subtracted from each of the raw spectrum and the reference spectrum prior to normalization. Subsequently, the data was analysed using a MATLAB Code that allowed us to first highlight the regions of high modulation in the relative transmission spectrum. This corresponded to the edges of the droplets. Using the information of the droplet edges, the time points corresponding to the droplet region and oil region were identified. It should be noted that through this analysis, we get the normalized transmission intensity as a function of wavelength and time.

Results and Discussion

In this work, we demonstrate the light interaction with anisotropic nanoparticles in non-spherical droplets using homemade optical spectroscopy which enables real time, non-invasive monitoring with high sensitivity. As mentioned earlier, isotropic drops are typically formed using microfluidic flow focusing geometries and require fluids to pass through a narrow neck as shown in Figure S1A of SI. As shown, oil flowing through channels marked 'a' and 'b', focusses the water, flowing in inlet marked 'c' through a narrow (50 µm) channel. For reactors containing reagents, this neck serves as a rapid diffusion zone for instantaneous reactions leading to uncontrolled fouling and flow disruption (Figure S1B, SI). Hence most drop-based chemistries prefer T-junction geometries, where there are no narrow channels to enable

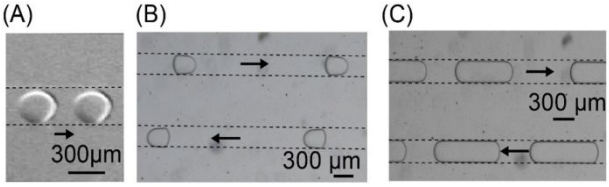

Figure 1 Stereomicroscopic images of **A.** Ellipsoidal droplets formed in flow-focusing geometry with R = 1 **B.** Bullet shaped droplets formed in T-junction geometry with R = 0.5. **C.** Capsule shape droplets formed in T-junction geometry with R = 1.2.

droplet breakup and the so-formed drops need not be isotropic as show in Figure 1. The ellipsoidal (almost isotropic) drops in Figure 1A were generated in our flow focusing microchannel, while the anisotropic drops in Figure 1B - C were generated in T-junction microchannel with R = 0.5 and 1.2 respectively. We also observed that the bullet shaped drops were not formed for $R > 0.75$. Since the nature of breakup at the junction determined by the flow ratios of the fluid in question and channel geometry also dictates the size and shape of the droplets formed (which essentially shows that the droplet shape is process dependant). Hence, we had no control over the shape of the drop formed during our nanoparticle synthesis within droplets.

Light scattering from single microfluidic droplets

Figure 2A shows the schematic of numerical modelling of light scattering by a droplet with an ideal cylindrical shape with hemispherical caps (blue). The forward scattered intensity is affected by the portion of the droplet illuminated by the light source. In the case when the extremities of the droplet are illuminated, refraction of light due to various incidence angles (with the surface) leads to significant scattering at high angles, and less intensity is directly transmitted. Figure 2B shows the light scattering intensity as a function of scattering angle and relative droplet position. This shows that when light is positioned at the ends of the droplets, light is scattered significantly. It is clear that only some of the scattered light can be collected which corresponds to the limits imposed by the NA of the collection objective. Figure 2C shows the images of light scattering for different positions of the droplets[52]. In the case where the beam diameter is smaller than the droplet size (l_L<<L), light scattering from the edges can be prominently

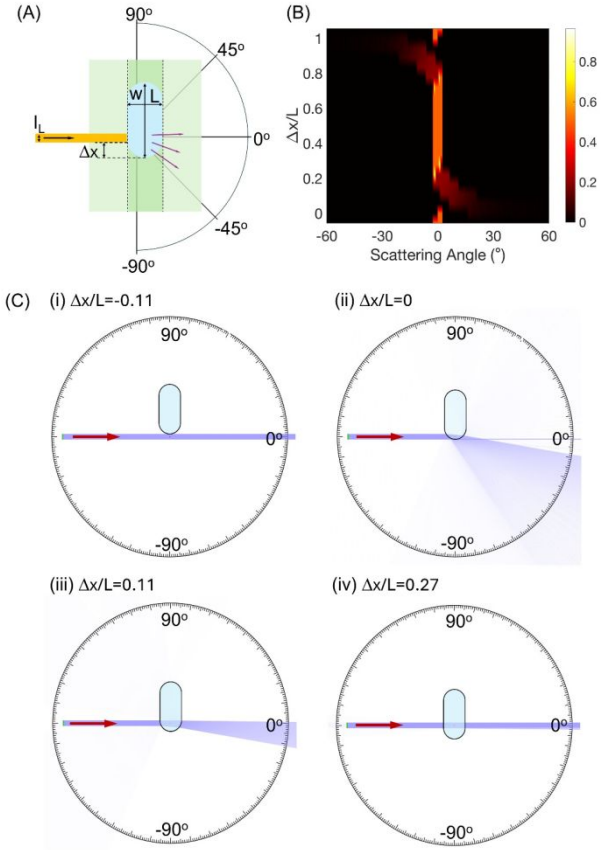

Figure 2: A. Schematic of the configuration used for understanding light scattering from single droplets. **B.** Relative scattering intensity (color) as a function of scattering angle and relative position of the drop (Δx/L). The beam size (l_L) and droplet width are kept fixed at 0.11 L and 0.44 L, respectively. **C.** Images showing the position dependent angular scattering of light by the single droplet[52].

Nanoscale Advances Accepted Manuscript

Please do not adjust margins

View Article Online
DOI: 10.1039/D5NA01087J

observed by measuring the forward scattered light. Additionally, once the beam traverses the curved ends of the

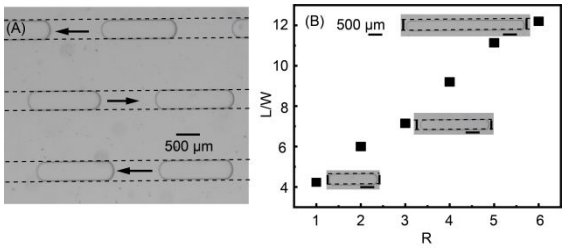

Figure 3: Droplet analysis using Stereomicroscope: **A.** Stereo microscopic image of droplet measured at a total flow rate of 7 µL/min where Q_o and Q_a were 4 and 3 µL/min, respectively **B.** Various droplet sizes measured at different flow rates, where L is the length of the drop, W is the width of the channel, and R is the ratio of Q_a/Q_o; insets show representative images of the drops.

drop, the light scattering is minimal at higher angles enabling monitoring of the different parts of the droplet. On contrary, in the case when the beam diameter is comparable to the droplet size (I_L~L), the measured signal in the forward scattered direction is a convolution of the signal scattered from the edges and from the flat part of the drop. This condition would provide an averaged signal from a single drop and information about the spatial variation of the signal is lost. From these analyses, it is clear that a judicious choice the illumination as well as the collection conditions is crucial for performing single-drop optical spectroscopic analysis. In the following sections, we use a homemade optical platform for carrying out single drop measurements. We used GNR as a representative system for validating the system.

Measuring the response of single droplets

We performed flow experiments to analyse the drop size with variations in R. Stereomicroscopic images taken using Nikon SMZ1270 (Figure 3A) were processed using ImageJ and their non-dimensional length (L/w, w being the channel width) was plotted against R (Figure 3B with insets showing a drop). The Q_a, Q_o and R for the drops in Figure 3A were 3, 4 µL/min and 0.75 respectively, thus leading to a capsule shaped drop of length ~ 1185 µm. As can be seen, as R increases, typically Q_a increases for constant Q_o, and the volume of the droplets transition from picolitres to nanolitres thus leading to an increase in drop size – length. Thus, as the R changes, the volume of the droplets and the final concentration of the reagents added into the drops varies as well. We then used the similar flow ratios to perform optical measurements using the in-house optical platform.

The schematic of the optical platform used for single droplet measurements is shown in Figure 4A. In this optical setup, we control the illumination and collection conditions. The condenser aperture is adjusted such that only a portion of the droplet is illuminated, limiting the volume from which the transmitted signal is collected. Furthermore, we use a 60X (0.7 NA) objective to collect both the directly transmitted light and forward scattered light within a light cone of 44°. We placed the microfluidic device (Figure 4A) between the objective and light source, on an adjustable (x, y, and z) stage and the light illumination was on the droplet. Figure 4B, shows the schematic of the microchannel where the droplet breakup occurs at the T-junction geometry. Silicon oil (orange) flows through the first inlet while an aqueous solution of surfactant, (CTAB, at 0.5 mM, its critical micelle concentration, blue) was injected through the other two inlets representing the dispersed phase. The images of the drops as captured using the inverted optical microscope camera, provided in Figure 4C shows (i) the trailing edge, (ii) drop centre and (iii) the leading edge of a single drop.

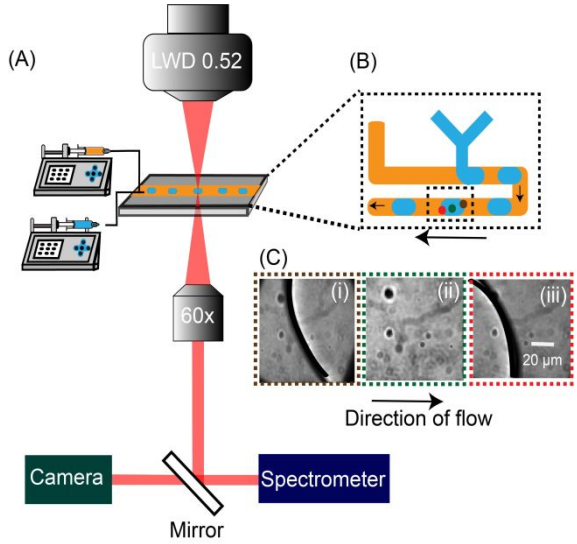

Figure 4: A. Schematic of the in-house optical setup used for single droplet spectroscopic measurements **B.** Schematic of microfluidic T-junction chip used to form droplets. **C.** Images obtained using the inverted optical microscope showing different locations of a single droplet highlighted in the panel B. **(i)** Brown dot shows the trailing edge **(ii)** Green dot the mid-section and **(iii)** Red dot the leading edge of the drop.

The captured raw data is shown in Figure 5A, a typical spectral plot showing the variation in the normalized transmission intensity as a function of wavelength and time. Using MATLAB, we analysed the spectra acquired in each experiment. This spectral plot of the captured data provided in Figure 5A can be interpreted as follows: the red regions of intensity ~ 1.05 correspond to the edges of the droplets due to increased scattering at the droplet boundaries. The centre of the drop containing water are indicated by the green regions where the intensities go down to ~ 0.95. The blue regions of intensities ~0.85 represent the oil phase, where light scattering is less than that of the droplet region (both the edges and the centre). This is due to the change in the refractive index of the water (1.33, CTAB =1.46) and oil (1.403).

Open Access Article. Published on 20 January 2026. Downloaded on 1/22/2026 7:56:22 AM.
This article is licensed under a Creative Commons Attribution-NonCommercial 3.0 Unported Licence.

Nanoscale Advances Accepted Manuscript

This journal is © The Royal Society of Chemistry 20xx

Please do not adjust margins

View Article Online
DOI: 10.1039/D5NA01071

Open Access Article. Published on 20 January 2026. Downloaded on 1/22/2026 7:56:22 AM.
This article is licensed under a Creative Commons Attribution-NonCommercial 4.0 Unported Licence.

Figure 5B shows the transmittance intensities as a function of time for a fixed wavelength. Because of the dynamic state of the droplets, the scattering of light interaction with the droplet changes even with the constant illumination of light throughout the experiment. This plot also shows the number of droplets generated within a 3s window for a specific flow rate. First, the data set analysed were grouped to cluster the spectra originating from the droplet region ("droplets-only") or from the continuous phase ("oil-only"). Due to large scattering at the oil-droplet interface, the transmitted signal depicts a large change in signal which we attribute to the interface. Figure 5B highlights the droplet and oil phase regions based on the system's transmittance levels. The transmittance value 1 represents the oil phase, and 1.04 and 1.05 depict the droplet preceding and leading-edge transmittance signals. This was confirmed by measuring the temporal cuts of the preceding and trailing edges of drop images from a stereomicroscope as shown in Figure S3 of SI. The front end of the drop shows lower counts as compared to the back end of the drop which directly corresponds to lower transmission spectrum at the front end of the drop. Comparing

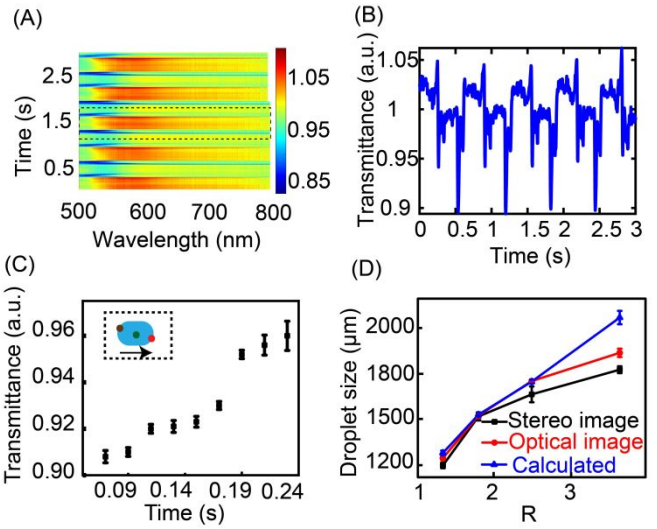

Figure 5: A. Droplet spectra plot using MATLAB and **B.** Discrete droplet analysis, showing the transmittance plotted as a function of time at 665 nm. **C.** Droplet transmittance profile plotted over time showing a distinct variation between the leading and trailing edges of the droplet using MATLAB data obtained from panel B. Inset shows the leading (red dot) and trailing edges (brown dot) on a single droplet. **D.** Comparison of droplet size among the images obtained from stereo, optical microscopes, and through data analysis from optical measurements.

this to the spectral data, we are able to assign the orientation of the drop (front and back) with the spectral time trace i.e. on comparing Figure 5C and Figure S3B, at 0.05 s, the lower transmittance of ~ 0.9 corresponds to a drop dimension of ~60 µm which is the leading front compared to the transmittance intensity (~ 0.96) at 0.24 s where the drop dimension is ~ 150 µm, the trailing end of the drop. In addition, we also compared the drop lengths calculated from stereomicroscopic images (black, closed circle, Figure 5D) and optical microscopic (red, closed circle, Figure 5D) images. We also used the captured videos (1s) from the microscopes and calculated the droplet lengths based on the velocity of the fluid and the elapsed time represented as calculated (blue closed triangle). This comparison between the stereo and inverted optical microscope images for a given time and drop size ensured the accuracy of our analysis.

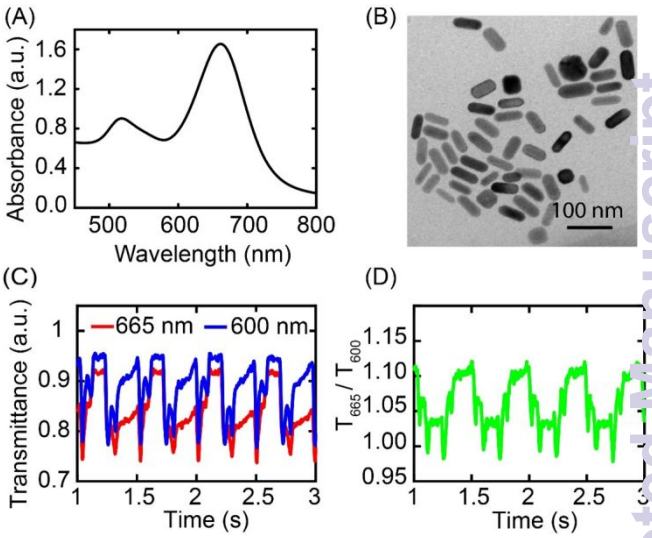

Figure 6: A. UV-Visible absorption spectrum of the GNR exhibiting a longitudinal LSPR at 665nm. **B.** Representative TEM image of the GNRs. **C.** Normalized transmission as a function of time at two different wavelengths, i.e., at 665 nm (resonance wavelength of GNR) and 600 nm (off-resonance wavelength) for 3 sec. **D.** The transmittance ratio between the two wavelengths noted in (panel C) to identify the intensity variation in the oil phase and GNR loaded droplet region.

As previously mentioned, changing R resulted in varying drop length 1.2 mm to 2 mm when R was varied from 1.3 to 3.4, respectively, as shown in Figure 5D. All three obtained plots show minimal variations at low R while the variations are significant at higher values of R because of the error in measurements of high-speed videos. Hence, we restricted our range of R to < 2 for further experiments. We hence performed experiments with a total flow rate of 4 µl/min with both Qa and Qo equal at 2 µl/min thus the droplet size was maintained at ~ 600 µm across experiments. The total volume of the aqueous sample in each droplet at such condition was 13 nL while the light illumination corresponds to a volume of around 3.4 nL achieved by adjusting the condenser aperture.

Analysis of GNR-loaded microdroplets

Since we are now able to recognize the 'droplet only' regions in the obtained raw data, we went on to identify the presence of GNR in the drops. To achieve this, we considered a series of total flow rates, i.e., 1, 4, and 7 µL/min, while maintaining a constant droplet size (~ 600 µm) as previous experiments by maintaining constant R at 1 and equal Q_o and Q_a across all experiments.

We then measured the transmittance spectra for each droplet obtained from various total flow rates for a fixed wavelength

Nanoscale Advances Accepted Manuscript

Please do not adjust margins

View Article Online
DOI: 10.1039/D5NA01087J

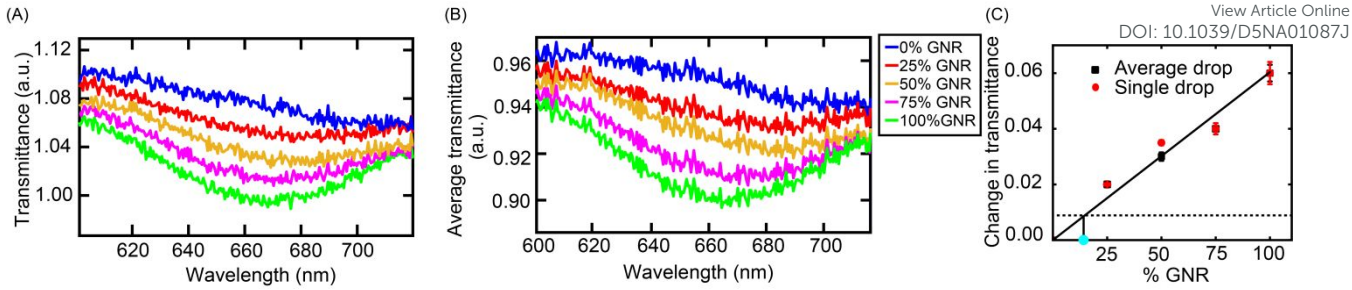

Figure 7. Dilution series of anisotropic gold nanoparticles: Plots showing the **A.** Transmittance as a function of wavelength as the concentration of GNR varies in a single drop. **B.** Transmittance vs. wavelength averaged across 28 droplets (8200 spectra) by eliminating the oil phase using MATLAB code. **C.** Plot of the change in transmittance to the GNR dilution obtained using both single droplet analysis and average droplet analysis. The dotted line represents the signal to noise ratio measured and averaged across all the single drop transmittance data which intersects the trendline (black line) at the least GNR dilution that can be detected using our system – blue dot at 13% GNR represents the limit of detection of our system.

region from 400-900 nm. Irrespective of total flow rate, we obtained flat transmission profile for water-containing droplets (Figure S4 of SI). Subsequently, we performed similar experiments where the aqueous fluid was replaced with GNR. These GNRs exhibit a longitudinal localized surface plasmon resonance (LSPR) peak at 665 nm with a strong absorbance of 1.6 a.u., as shown in Figure 6A. A representative TEM image of the GNRs, is shown in Figure 6B, showing a nominal aspect ratio of 2.6±1.3. Since the GNRs exhibit a strong absorbance at 665 nm due to their LSPR, we were able to capture their signal effectively at all 3 total flowrates tested as shown in Figure S5 SI. However, we observed that lower flow rates (i.e., reduced droplet velocity) produced significantly higher optical transmission signals compared to higher flow rates (i.e., faster droplet velocity). This behaviour can be attributed to a decrease in the interfacial tension between the aqueous and oil phases, which is inversely proportional to the flow velocity. As the flow velocity increases, the interfacial tension decreases, leading to weaker scattering and absorption signals and signal clarity[28]. Hence, we used an intermediate total flow rate of 4 µL/min for further experiments.

To further quantify the GNR contribution, we considered two wavelength values: 665 nm, resonance wavelength, and 600 nm, off-resonance wavelength and did the comparative spectral analysis. The obtained transmittance as a function of time is shown in Figure 6C, at 665 nm (red, resonant) and 600 nm (blue, off-resonance). The change in transmittance between two wavelengths in the 'droplet only' region is 0.08 (Figure 6D), while the change in transmittance between the two wavelengths in the 'oil only' region is 0.02. This pronounced variation in transmittance between the two wavelengths in the 'drop only' region compared to the 'oil only' region indicates the presence of GNR in the 'drops only' region i.e. the optical signatures of the GNRs at 665 nm in the drops as against their absence in the oil.

Dilution of GNR concentration in a single droplet

After identifying GNRs in the 'drop only' region, we further performed dilution experiments to investigate the effects of varying GNR concentrations within individual droplets. We achieved this by adding water and GNR into the droplet. These experiments were performed for the same flow condition as previous experiments with water in one of the inlets and GNR in the other inlet for dispersed phase as shown in Figure S2 of SI. We first performed water-only experiments with the GNR inlet blocked and water inlet at 2 µL/min, corresponding to a 0% GNR concentration. For subsequent measurements, the water flow rate was reduced to 1.5 µL/min, while the GNR flow rate was increased to 0.5 µL/min, corresponding to a 25% GNR concentration. The experiments were then conducted at 50%, 75%, and 100% GNR concentrations by adjusting the flow rates of water and GNR while maintaining a constant droplet size across all experiments. The analysed data is shown in Figure 7; Figure 7A is a plot of the transmittance spectrum of single droplet at various GNR concentrations. The blue line represents the baseline, 0% GNR concentration (i.e., 100% water), resulting in a flat transmission profile. As the GNR concentration increased from 0% to 100%, a continuous shift in the transmittance spectrum was observed, with a notable increase in the depth of the absorption at the longitudinal peak (665 nm), indicating the increasing absorbance of the GNR within the droplet. This trend highlights the direct correlation between GNR concentration and transmittance changes. Figure 7B depicts the average transmittance spectrum for all droplets in the experiment. This analysis revealed that there was minimal variation between the individual droplet measurements and the average values across all droplets. The average values, calculated from data analysis of all the droplet data, confirm the overall trends observed in single droplets but smooth out the variations between droplets, providing a broader view of the effects of GNR concentration. In Figure 7C, we present the comparison between the average and the single droplet transmittance data. This comparative analysis further confirms that the transmittance changes are primarily due to the presence of GNR particles within the droplets, and

Open Access Article. Published on 20 January 2026. Downloaded on 1/22/2026 7:56:22 AM.
This article is licensed under a Creative Commons Attribution-NonCommercial 3.0 Unported Licence.

Nanoscale Advances Accepted Manuscript

This journal is © The Royal Society of Chemistry 20xx

View Article Online
DOI: 10.1039/D5NA01087J

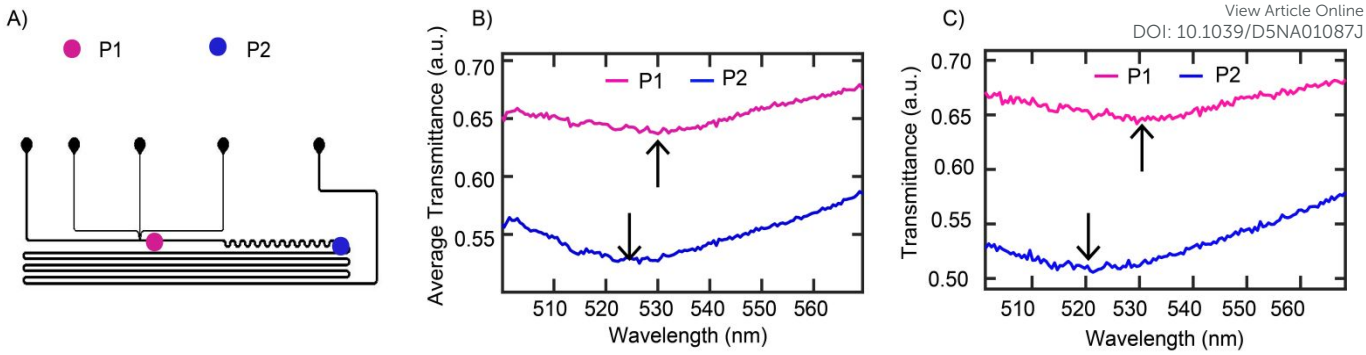

Figure 8. Influence of measurement location on the synthesis of gold nanoparticles (Case 1): **A.** Schematic of the microfluidic T junction device showing 2 locations P1 and P2, where spectral measurements were taken, to indicate the formation of gold nanoparticle. Plots of **B.** Transmittance as a function of wavelength in a single drop and **C.** Transmittance as a function of wavelength as the formation of gold nanoparticles varies averaged over all drops

it quantifies the spectral shift across different GNR concentrations. We then plotted the S/N line on this curve (black dotted line) in order to determine the limit of detection of our system. The S/N was measured and averaged across all the single drop transmittance data and the limit of detection (LoD) of our system was determined to be the GNR dilution at which the S/N intersected the change in transmittance which was ~ 13% corresponding to a GNR concentration of 8.3 x 10^8.

Real-time monitoring of *in-situ* synthesis of gold nanoparticles within droplets

We conducted a detailed analysis of gold nanoparticle synthesis through single-droplet measurements using two distinct cases of experiments. In the first case, we examined spatial effects by shifting the droplet's position by a few centimetres to monitor *in-situ* changes during the reaction. In the second case, we investigated the impact of varying reactant concentrations within a single droplet at a fixed location along the channel. We have included a third case where we try to analyse the data obtained from similar experiments using a FF geometry (as shown in Figure S1A – S1F). To mitigate the fouling issues associated with this geometry, a T-junction configuration was preferred for the synthesis of gold nanoparticles.

Case 1: Influence of measurement location on the synthesis of gold nanoparticles (GNP)

For the first set of experiments, the microfluidic device was configured with two inlets for the dispersed phase: one for the gold precursor solution and one for ascorbic acid (1M of AA) as shown in Figure S6A of SI. Upon convergence of the gold precursor and ascorbic acid streams into the droplet, rapid mixing led to reaction and formation of GNP almost instantaneously. The first measurement was taken at the T junction where drops are formed, marked P1 in Figure 8A, and the second was taken downstream (~ 2.7 cm length of the channel), at location P2, in order to observe changes over the time. We measured the spectral transmission from a single drop as well as calculated the average transmission over 15 drops as shown in Figure 8B and 8C. Note that the transmission dip at 523 nm indicates the formation of *spherical GNP* and the intensity is proportional to the concentration of the GNP.

Figure 8B, shows a dip of 0.65 a.u. at 523 nm indicating lower concentration of GNP at location P1 (pink). At location P2 (blue), the transmission of droplet is lower (~ 0.51 a.u.) showing a prominent dip, indicating higher density of particles. This significant increase in absorbance (decrease in transmittance in the Figure 8B) at location P2 confirms the progressive nanoparticle growth within the moving droplets as the droplets traverse the channel. This spatial difference underscores the effectiveness of our microfluidic approach in capturing the real-time evolution of nanoparticle synthesis. A comparison of Figures 8B and C indicates that both single drop spectra and average spectra show similar variations in the transmission intensity.

Case 2: Variation in the concentration of AA

To demonstrate that this technique is able to track changes in the nanoparticle synthesis, we performed the real-time measurements at a fixed location along the channel length for two different concentrations of the reducing agent (AA). The microfluidic device was configured with three inlets for the dispersed phase: one for the gold precursor solution, one for ascorbic acid (1M of AA), and a third for water, which was either open or closed depending on the experimental requirement as shown in Figure S6B of SI.

We measured the transmission spectra at the T-junction as shown by black dot in Figure 9A. We started with 1 M AA concentration (blue in Figure 9B) and the measured spectra exhibits a dip at 535nm (~ 0.76 a.u.). Subsequently, we introduced water through the third inlet to tune the AA concentration to 0.5 M and the spectral signature is shown as pink in Figures 9B. A lower transmittance value of ~ 0.85 a.u. at peak wavelength of 535 nm at lower AA concentration indicates the formation of gold nanoparticles albeit lower

Open Access Article. Published on 20 January 2026. Downloaded on 1/22/2026 7:56:22 AM.
This article is licensed under a Creative Commons Attribution-NonCommercial 3.0 Unported Licence.

Nanoscale Advances Accepted Manuscript

View Article Online
DOI: 10.1039/D5NA01087J

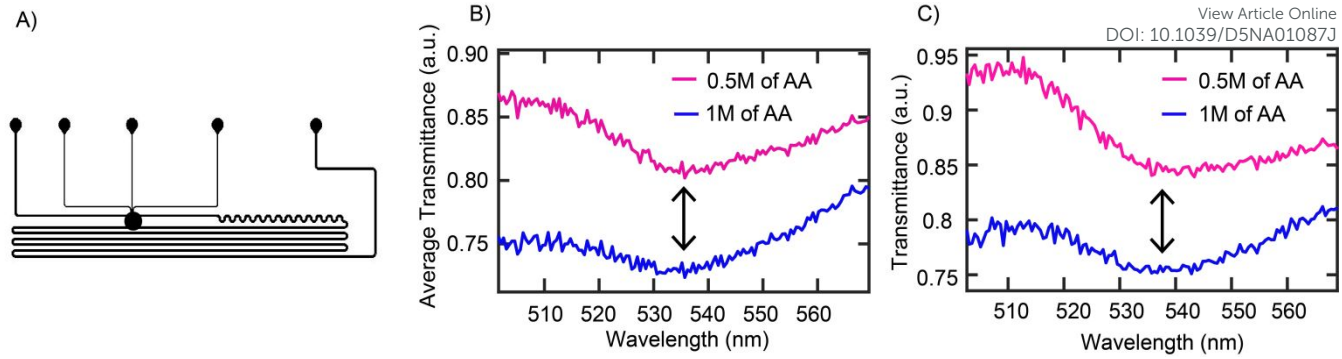

Figure 9. Variation in the concentration of AA (Case 2): A. Schematic of the microfluidic T junction device showing the location at which the spectral measurements were taken, to indicate the formation of gold nanoparticle. Plots of **B.** Transmittance as a function of wavelength in a single drop and **C.** Transmittance as a function of wavelength as the formation of gold nanoparticles varies averaged over all drops

concentration due to low availability of the reducing agent i.e. for lower concentrations of AA, the reduction of the gold salt is less leading to lower density of particles formed within the droplets. A clear difference in the reaction dynamics is observed due to change in the concentration of AA. Furthermore, spectra from individual and averaged droplets show negligible differences indicating the uniformity of the particles synthesized in the train of droplets. Using these two cases, we demonstrate real-time measurements of on-chip synthesis of the gold nanoparticle with our in-house optical setup.

Case 3: Flow focussing device for GNP synthesis

We performed a few experiments using a flow focusing device shown in Figure S1A within spherical droplets and tried to measure the transmission signals at the junction where the drops form. The spectral plot shown in Figures S7A, indicates fouling in the channel (red) which results in improper identification of droplets i.e. the leading and trailing edge of the droplets were not differentiated correctly (Figure S7B at 530 nm). Due to channel fouling, the drop edges could not be clearly defined.

The optical interrogation method developed here demonstrates that the optical response from single drops can be measured with high sensitivity even when there are no fluorescence or Raman markers within the droplets. Note that the measured contrast originates from the absorption of the gold nanorods and can be extended to any other system which exhibits absorption in the visible spectral region. Thus, this technique can potentially be used for all sorts of absorbing dyes, employed for biochemical assays, and other nanomaterials and nanoparticles[53–55]. The temporal resolution of this technique is limited by the data acquisition time of the spectrometer. The speed can be further increased by reducing the number of pixels of the CCD camera from the integration is performed. Employing this, it is possible to record a spectrum every 30 µs. However, this reduction in the acquisition time also leads to a reduction in the S/N ratio of the acquired spectrum. Thus, depending on the expected modulation of the absorbance in an experiment, a judicious choice of the integration time per spectra and the S/N needs to be made. Furthermore, light sources with different wavelengths (for example, in the UV range) can be used for looking at proteins and DNA within single droplets and have potential implications for real-time single drop PCR analysis[56–59].

Conclusions

In conclusion, we developed a technique for the single drop analysis using an in-house custom-built optical transmission spectroscopy setup integrated with a 'T' junction-based droplet microfluidic device. Using the understanding of light scattering from the droplets, we employ a MATLAB code to analyse the 5000-8000 spectra from a single flow condition and identify the spectra corresponding to the 'droplet only' region. We compare the stereomicroscopic images, optical microscope images to validate the 'drop only' and 'oil only' regions identified by spectral data analysis. We then interrogated individual droplets loaded with gold nanorods and measured their transmission spectral signatures. We also varied the concentration of AuNRs within the droplets to demonstrate the sensitivity of the single-drop measurement. On comparing the single drop data with the multi-drop averaged data, we show that the signatures of the nanorods are retained even at the single drop analysis, however the S/N ratio is improved on averaging. Finally, we demonstrated the real-time monitoring of in-situ synthesis of gold nanoparticles within a single droplet. We showed that by varying the location of measurement along the channel length, it is possible to track the reaction timeline. We also showed the influence of reactant concentrations on the nanoparticle synthesis for at a fixed position, vis-à-vis, a fixed reaction time. We envision that the established method can be used for in-situ monitoring of most chemistry and bio-chemical assay exhibiting a change in

Open Access Article. Published on 20 January 2026. Downloaded on 1/22/2026 7:56:22 AM.
This article is licensed under a Creative Commons Attribution-NonCommercial 3.0 Unported Licence.

Nanoscale Advances Accepted Manuscript

This journal is © The Royal Society of Chemistry 20xx

the transmission signal of the solution within a single droplet over a wide spectral range.

View Article Online
DOI: 10.1039/D5NA01087J

Open Access Article. Published on 20 January 2026. Downloaded on 1/22/2026 7:56:22 AM.
This article is licensed under a Creative Commons Attribution-NonCommercial 3.0 Unported Licence.

Nanoscale Advances Accepted Manuscript

Author contributions

R.P. carried out the experiments, prepared the manuscript, and assisted in the discussions; J.P. assisted in the experiments and assisted in manuscript preparation; S.D.-G. and S. D. jointly conceived the idea, assisted in manuscript preparation, and assisted in the discussions.

Conflicts of interest

The authors have no known conflict of interests concerning the publication of this research.

Data availability

The data supporting this article have been included as part of the Supplementary Information.

Acknowledgements

The authors would like to acknowledge financial support from Ministry of Education granted to RP, Seed research grant from Indian Institute of Technology Hyderabad (IITH/Seed Grant/2020-2021/F222/SG17) and Start-up research grant from SERB-SRG (SRG/2021/001623) granted to SD. SDG would like to acknowledge funding support from the TDG Grant of IIT Hyderabad (TDG/IITH/F199/2024-25/TDG-08), SERB Ramanujan Grant (SB/S2/RJN-126/2017) and DST Nanomission Grant (DST/NM/NB/2018/118).

References

1 H. Song and R. F. Ismagilov, *J Am Chem Soc*, 2003, **125**, 14613–14619.
2 Hindson *et al.*, *Anal Chem*, 2011, **83**, 8604–8610.
3 Y. Schaerli and F. Hollfelder, *Mol Biosyst*, 2009, **5**, 1392.
4 R. L. Hartman and K. F. Jensen, *Lab Chip*, 2009, **9**, 2495.
5 T. Moragues, D. Arguijo, T. Beneyton, C. Modavi, K. Simutis, A. R. Abate, J.-C. Baret, A. J. deMello, D. Densmore and A. D. Griffiths, *Nat Rev Methods Primers*, 2023, **3**, 32.
6 S. Sart, G. Ronteix, S. Jain, G. Amselem and C. N. Baroud, *Chem Rev*, 2022, **122**, 7061–7096.
7 Y. Yang, C. Li, J. Kameoka, K. H. Lee and H. G. Craighead, *Lab Chip*, 2005, **5**, 869.
8 S. Li, C. Zhang, S. Wang, Q. Liu, H. Feng, X. Ma and J. Guo, *Anal*, 2018, **143**, 4230–4246.
9 B. Kuswandi, Nuriman, J. Huskens and W. Verboom, *Anal Chim Acta*, 2007, **601**, 141–155.
10 Y.-J. Wei, Y.-N. Zhao, X. Zhang, X. Wei, M.-L. Chen and X.-W. Chen, *TrAC*, 2023, **158**, 116865.
11 Y. Liu, Z. Fan, L. Qiao and B. Liu, *TrAC Trends in Anal Chem*, 2022, **157**, 116822.
12 Z. Fattahi and M. Hasanzadeh, *TrAC Trends in Anal Chem*, 2022, **152**, 116637.
13 J. Pillanagrovi and S. Dutta-Gupta, *Nano Futures*, 2024, **8**, 045001.
14 E. Mukherjee, J. Pillanagrovi, D. Bhatnagar and S. Dutta-Gupta, *J Appl Phys*, DOI:10.1063/5.0132791.
15 S. Dutta-Gupta, N. Dabidian, I. Kholmanov, M. A. Belkin and G. Shvets, *Phil Trans R Soc A* , 2017, **375**, 20160061.
16 J. Pillanagrovi and S. Dutta-Gupta, *Nanotechnol*, 2022, **33**, 485301.
17 G. Kelp, J. Li, J. Lu, N. DiNapoli, R. Delgado, C. Liu, D. Fan, S. Dutta-Gupta and G. Shvets, *Lab Chip*, 2020, **20**, 2136–2153.
18 N. Dabidian, S. Dutta-Gupta, I. Kholmanov, K. Lai, F. Lu, J. Lee, M. Jin, S. Trendafilov, A. Khanikaev, B. Fallahazad, E. Tutuc, M. A. Belkin and G. Shvets, *Nano Lett*, 2016, **16**, 3607–3615.
19 J. P. Neto, A. Mota, G. Lopes, B. J. Coelho, J. Frazão, A. T. Moura, B. Oliveira, B. Sieira, J. Fernandes, E. Fortunato, R. Martins, R. Igreja, P. V. Baptista and H. Águas, *Lab Chip*, 2023, **23**, 3238–3244.
20 S. R. T. Neil, C. M. Rushworth, C. Vallance and S. R. Mackenzie, *Lab Chip*, 2011, **11**, 3953.
21 M. Li, F. Zhao, J. Zeng, J. Qi, J. Lu and W.-C. Shih, *J Biomed Opt*, 2014, **19**, 111611.
22 H. Zhang, Y. Yi, C. Zhou, G. Ying, X. Zhou, C. Fu, Y. Zhu and Y. Shen, *RSC Adv*, 2017, **7**, 52782–52793.
23 X. Casadevall i Solvas, X. Niu, K. Leeper, S. Cho, S.-I. Chang, J. B. Edel and A. J. deMello, *JoVE*, DOI:10.3791/3437.
24 P. Gupta, A. Mohan, A. Mishra, A. Nair, N. Chowdhury, D. Balekai, K. Rai, A. Prabhakar and T. Saiyed, *Microsyst Nanoeng*, 2024, **10**, 35.
25 M. P. Cecchini, J. Hong, C. Lim, J. Choo, T. Albrecht, A. J. deMello and J. B. Edel, *Anal Chem*, 2011, **83**, 3076–3081.
26 M. P. Cecchini, A. Wiener, V. A. Turek, H. Chon, S. Lee, A. P. Ivanov, D. W. McComb, J. Choo, T. Albrecht, S. A. Maier and J. B. Edel, *Nano Lett*, 2013, **13**, 4602–4609.
27 M. Srisa-Art, A. J. deMello and J. B. Edel, *Phys Rev Lett*, 2008, **101**, 014502.
28 T. D. Rane, C. M. Puleo, K. J. Liu, Y. Zhang, A. P. Lee and T. H. Wang, *Lab Chip*, 2010, **10**, 161–164.
29 V. Srinivasan, V. K. Pamula and R. B. Fair, *Anal Chim Acta*, 2004, **507**, 145–150.
30 A. Zinchenko, S. R. A. Devenish, B. Kintses, P.-Y. Colin, M. Fischlechner and F. Hollfelder, *Anal Chem*, 2014, **86**, 2526–2533.
31 S. Hassan, A. M. Nightingale and X. Niu, *Anal*, 2016, **141**, 3266–3273.
32 T. A. Duncombe, A. Ponti, F. P. Seebeck and P. S. Dittrich, *Anal Chem*, 2021, **93**, 13008–13013.
33 J. Probst, P. Howes, P. Arosio, S. Stavrakis and A. deMello, *Anal Chem*, 2021, **93**, 7673–7681.
34 M. Sulliger, J. Ortega Arroyo and R. Quidant, *Anal Chem*, 2025, **97**, 2736–2744.
35 R. R. Pompano, W. Liu, W. Du and R. F. Ismagilov, *Annu Revi Anal Chem*, 2011, **4**, 59–81.
36 T. Thorsen, R. W. Roberts, F. H. Arnold and S. R. Quake, *Phys Rev Lett*, 2001, **86**, 4163–4166.
37 A. Venkateshwarlu and R. P. Bharti, *J Taiwan Inst Chem Eng*, 2021, **129**, 64–79.
38 S. L. Anna, N. Bontoux and H. A. Stone, *Appl Phys Lett*, 2003, **82**, 364–366.
39 A. Ghosh, S. Ghosh, F. Pati and S. Duraiswamy, *Bioprinting*, 2023, **36**, e00316.
40 Sourita ghosh, Amith Ghosh, Falguni Pati and Suhanya Duraiswamy, *ACS Biomater Sci Eng*.
41 Y. Mahdi and K. Daoud, *J Dispers Sci Technol*, 2017, **38**, 1501–1508.
42 A. Gupta and R. Kumar, *Phys Fluids*, DOI:10.1063/1.3523483.
43 S. Duraiswamy and S. A. Khan, *Small*, 2009, **5**, 2828–2834.
44 S. K. Jena, T. Srivastava, S. S. Bahga and S. Kondaraju, *Phys Fluids*, DOI:10.1063/5.0134087.
45 W. Han and X. Chen, *J Braz Soc Mech Sci* , 2021, **43**, 247.
46 A. Gupta and R. Kumar, *Microfluid Nanofluid*, 2010, **8**, 799–812.
47 S. A. Khan and S. Duraiswamy, *Lab Chip*, 2009, **9**, 1840.

View Article Online
DOI: 10.1039/D5NA01087J

48 Z. Barikbin, Md. T. Rahman, P. Parthiban, A. S. Rane, V. Jain, S. Duraiswamy, S. H. S. Lee and S. A. Khan, *Lab Chip*, 2010, **10**, 2458.
49 S. Duraiswamy and S. A. Khan, *Nano Lett*, 2010, **10**, 3757–3763.
50 L. Zanini and C. Sada, *Phys Fluids*, DOI:10.1063/5.0138475.
51 B. Nikoobakht and M. A. El-Sayed, *Chem Mater*, 2003, **15**, 1957–1962.
52 Ray Optics Simulations, https://phydemo.app/ray-optics/ (Oct 2025)
53 S. Hengoju, O. Shvydkiv, M. Tovar, M. Roth and M. A. Rosenbaum, *Biosens Bioelectron*, 2022, **200**, 113910.
54 E. Y. Basova and F. Foret, *Anal*, 2015, **140**, 22–38.
55 C. Ma, Z. Gao, J. Zhao and S. Feng, *NPE*, DOI:10.1063/10.0019677.
56 Y. Hou, S. Chen, Y. Zheng, X. Zheng and J.-M. Lin, *TrAC* , 2023, **158**, 116897.
57 N. R. Beer, B. J. Hindson, E. K. Wheeler, S. B. Hall, K. A. Rose, I. M. Kennedy and B. W. Colston, *Anal Chem*, 2007, **79**, 8471–8475.
58 W. Zhang, L. Cui, Y. Wang, Z. Xie, Y. Wei, S. Zhu, M. Nawaz, W.-C. Mak, H.-P. Ho, D. Gu and S. Zeng, *Biosens J (Basel)*, 2023, **14**, 2.
59 M.Born and E.Wolf, Principles of Optics, Cambridge University Press, 1999.

Open Access Article. Published on 20 January 2026. Downloaded on 1/22/2026 7:56:22 AM.
This article is licensed under a Creative Commons Attribution-NonCommercial 3.0 Unported Licence.

Nanoscale Advances Accepted Manuscript

This journal is © The Royal Society of Chemistry 20xx

View Article Online
DOI: 10.1039/D5NA01087J

Real-Time Optical Spectroscopy for *In-Situ* Single Droplet Analysis

Rama Pandillapally[a], Pillanagrovi Jayakumar [b], Shourya Dutta-Gupta[b*] and Suhanya Duraiswamy[a*]

[a.] *Chemical Engineering, Indian Institute of Technology Hyderabad, Sangareddy 502284, Telangana, India*
[b.] *Materials Science and Metallurgical Engineering, Indian Institute of Technology Hyderabad, Sangareddy 502284, Telangana, India*

*Corresponding author email: shourya@msme.iith.ac.in and suhanya@che.iith.ac.in

The datasets supporting this article have been uploaded as part of the supplementary information.

Open Access Article. Published on 20 January 2026. Downloaded on 1/22/2026 7:56:22 AM.
This article is licensed under a Creative Commons Attribution-NonCommercial 3.0 Unported Licence.

Nanoscale Advances Accepted Manuscript